Contents lists available at ScienceDirect

Applied Catalysis B: Environmental

Low-temperature methanol dehydration to dimethyl ether over various small-pore zeolites

Dilshad Masih [a,b], Sohrab Rohani [b], Junko N. Kondo [a], Takashi Tatsumi [a,*]

[a] Global Edge Institute and Chemical Resources Laboratory, Tokyo Institute of Technology, 4259 Nagatsuta, Midori-ku, Yokohama 226-8503, Japan
[b] Department of Chemical & Biochemical Engineering, University of Western Ontario, London, ON, Canada

ARTICLE INFO

ABSTRACT

Eight-membered ring small-pore zeolites Rho and KFI have been synthesized, characterized and tested for dehydration of methanol to dimethyl ether at low-temperature, and compared with other zeolites and three different samples of γ-Al$_2$O$_3$. Both the zeolites were mainly crystallized from the synthesis gels with the Si/Al ratio of 5.0 by a conventional hydrothermal method without any agitation. The amount of total solid-acid sites was 1.65 mmol g^{-1} and 2.53 mmol g^{-1} for zeolite KFI and Rho, respectively. In addition, zeolites SSZ-13, RUB-13, and ZSM-5 were also employed for the reaction. Reaction conditions were optimized for a low-temperature catalytic dehydration of methanol selectively to dimethyl ether. Methanol dehydration efficiency of various zeolitic frameworks is discussed against the strength of solid-acidity, type of channel structure, specific surface area, and particle size. At temperatures $\leq 200\,^\circ$C, the overall catalytic efficiency of the small-pore zeolites with appropriate medium-strong acidity and 3-D channels was superior to that of the reference γ-Al$_2$O$_3$ materials.

© 2017 Elsevier B.V. All rights reserved.

1. Introduction

Dimethyl ether (DME) is a valuable energy carrier and recently gaining increased interests especially for its environmentally benign properties [1–3]. Since the past few years, direct production of DME from syngas and via dehydration of methanol has been getting a lot of attention. DME has many important industrial and household uses. Furthermore, it is an important intermediate for the production of a variety of chemicals and it is adequate to replace the notorious chlorofluorocarbons. Particularly, it has a good prospect for an ultra-clean next-generation synthetic fuel for diesel engines with zero level SO$_X$, lower NO$_X$ and smoke emissions. Hence, it can play a significant role to mitigate adverse climate changes [2]. Catalytic dehydration of methanol is one of the main routes for the production of DME [1]. Methanol is obtained from various under-utilized and renewable resources e. g. natural gas, coal, and biomass. Recently, the valorization of methanol is attracting a lot of attention for it is an alternate feedstock for the production of useful chemicals e. g. olefins and DME. Various solid-acid materials namely zeolites and γ-Al$_2$O$_3$ are used for the production of DME. In the ever changing geopolitical and economic situations, and in order to lessen dependence on petroleum, the methanol dehydration process to DME offers an attractive route to a sustainable production of a cleaner synthetic fuel.

Zeolitic materials are important solid-acid catalysts for a variety of heterogeneous catalytic reactions. Particularly, the extent and strength of solid-acid sites on a material are important factors in controlling catalytic dehydration reaction [3]. Since the discovery of methanol conversion to hydrocarbons over ZSM-5 (MFI-type zeolite), a number of studies have been devoted to the search of effective catalytic materials for the valorization of methanol [1–5]. Owing to their appropriate solid-acid properties, several zeolitic materials such as ZSM-5, SAPO-34, SAPO-46, AlPO-4, Linde W, Y, mordenite, ferrierite, beta, and clinoptilolite have been reported to be active for the dehydration of methanol [1,6–12]. Among the zeolites, ZSM-5 is one of the most studied and the best catalyst reported for this reaction. Besides methanol dehydration reaction, ZSM-5 along with SAPO-34 is the most extensively studied zeolitic material for methanol-to-olefins (MTO) reaction [1–3]. Formation of products other than DME and deposition of coke are two serious issues for the dehydration reaction carried out at high temperature. On the other hand, when the reaction is performed at low-temperature, achieving an adequate conversion of methanol and removal of the by-product, water, are two main challenging tasks. For a low-temperature methanol dehydration reaction, materials with strong Lewis acidity e. g. bare γ-Al$_2$O$_3$ exhibit poor activity because of the poisoning of active sites by water adsorption [13]. On the other hand, materials having strong Bronsted acidity e. g. protonated ZSM-5 and zeolite Y demonstrate high activity

---

* Corresponding author.
  E-mail address: ttatsumi@cat.res.titech.ac.jp (T. Tatsumi).

but were prone to produce secondary products like hydrocarbons and ultimately cause coke deposition [12,13]. In principal, a better resistance to the deposition of heavy hydrocarbons and an adequate removal of the equimolar water produced in the methanol dehydration reaction are important factors for the optimum performance of a particular catalyst.

Among zeolitic frameworks, eight-membered ring (8-MR), small-pore zeolites with appropriate solid-acid properties are potential candidates for the conversion of methanol to various chemicals. In addition to KFI and Rho, two other small-pore zeolites SSZ-13 (a CHA-type analog of SAPO-34) and RUB-13 were also examined for the dehydration reaction. These zeolites have a 3-dimensional (3-D) porous structure consisting of intersecting 8-MR channels except for the zeolite RUB-13 that has a 2-dimensional (2-D) network. SSZ-13 and RUB-13 have been reported for the related MTO reaction by Zhu et al. [14], and Yokoi et al. [15], respectively. Previously, we have presented a study on MTO reaction over Rho zeolite [16]. Detailed investigations on low-temperature methanol reaction over zeolites and comparison with γ-Al_2O_3 will provide a better understanding of the catalytic dehydration process towards development of practicable catalyst material.

The main zeolites under investigations, KFI and Rho both have comparable framework densities and a 3-D network of channels (Table S1) [17]. Thus, a comparison of the methanol dehydration process over these zeolite candidates with similar physicochemical and structural properties would be interesting. Rho zeolite has a typical composition of $Na_{6.8}Cs_{3.0}[Al_{9.8}Si_{38.2}O_{96}] \cdot 29H_2O$ and intersecting 8-MR (3.6 Å $\times$ 3.6 Å) channels [17]. Intensive studies were conducted on the RHO-type framework of zeolites for the synthesis of methylamines [18]. Besides our previous study [16], recently Ji et al. investigated on steam-dealuminated RHO-type zeolite for the MTO reaction [19]. Herein, we have extended the use of the zeolite Rho to this important methanol dehydration reaction. KFI zeolite has a typical composition of $K_{18}Sr[Al_{20}Si_{76}O_{192}] \cdot 72H_2O \cdot (18$-crown-6) and intersecting 8-MR (3.9 Å $\times$ 3.9 Å) channels [17]. KFI-type zeolite has been reported for sorption and catalytic reactions including MTO, but no detailed study exists on its catalytic use for the production of DME [19]. In addition to Rho and KFI, two other 8-MR zeolites, SSZ-13 and RUB-13 were also employed for the dehydration reaction. Here in, we are reporting an extensive study on low-temperature methanol dehydration over various small-pore zeolites and validating their catalytic efficiency against ZSM-5 and three different samples of γ-Al_2O_3.

2. Experimental

2.1. Preparation of catalysts

The zeolite materials were synthesized under hydrothermal conditions by following the reported recipes [17]. X-ray diffraction (XRD), scanning electron microscopy (SEM), and other instrumental analyses were performed to evaluate phase-purity of the obtained topologies and crystalline morphologies. A detailed elucidation of their other physicochemical properties was important in determining their potential use for this methanol dehydration reaction. For a typical synthesis of Rho zeolite without using a structure directing agent (SDA), first of all, $Al(OH)_3$ (Wako, Japan) was dissolved in an aqueous solution of NaOH (Wako, Japan) by refluxing at 100 °C. The obtained clear solution was taken in a Teflon beaker and cooled to room temperature (RT). Then an aqueous solution of $CsOH \cdot H_2O$ (Alfa Aesar, US) was added under stirring. Finally, a homogeneous synthesis gel was obtained with a slow addition of colloidal silica AS-40 (40% SiO_2, Aldrich, Japan) under vigorous stirring. The Si/Al ratio of the gel was 5.0 with a batch composition of $1.8Na_2O:0.3CsO:1.0Al_2O_3:10SiO_2:100H_2O$. Thus obtained gel was

homogenized for 2 h by stirring and then taken in a polypropylene bottle. Hydrothermal crystallization in a pre-heated oven was carried out for 10 days at 80 °C without any agitation. Besides this gel with Si/Al ratio of 5.0, other synthesis gels with Si/Al ratios of 10 and 20 were also prepared and put for crystallization of RHO-type zeolite. At the end of the crystallization process, the solid product was separated by vacuum filtration, washed with water and dried at 70 °C.

For the synthesis of KFI zeolite, at first $Al(OH)_3$ was dissolved in an aqueous solution of KOH (Wako, Japan) under reflux at 100 °C. After cooling down the solution to RT, the obtained clear solution was poured into a Teflon beaker and mixed with an aqueous solution of $SrCl_2 \cdot 6H_2O$ (Aldrich, Japan), and 18-crown-6 (Wako, Japan) under stirring. The colloidal silica AS-40 was slowly added to the reaction mixture under vigorous stirring to achieve a homogeneous synthesis-gel. The Si/Al ratio of the synthesis gel was kept at 5.0 with a batch composition of $2.3K_2O:0.1SrO:1.0Al_2O_3:10SiO_2:220H_2O:1.0(18$-crown-6). The obtained synthesis gel was further stirred for 0.5 h and then taken in a Teflon vessel and enclosed in a steel bomb. Hydrothermal crystallization under static conditions was carried out for 120 h at 150 °C in a pre-heated oven. The product obtained at the end of the crystallization reaction was separated by vacuum filtration, washed with water and dried at 70 °C. The organic SDA (18-crown-6) in the KFI zeolite was removed by calcination of the as-obtained product at 550 °C. Detailed synthesis and characterizations of SSZ-13 and RUB-13 are found in the reported studies [14,15].

To obtain proton-type solid-acid zeolite catalyst for the methanol dehydration reaction, at first, the counter cations in the zeolite were exchanged with ammonium ions by repeated interactions with aqueous phase NH_4Cl (Wako, Japan). For a typical cation-exchange reaction, 1.0 g of the as-prepared zeolite powder was added into 100 ml aqueous solution of 1 M NH_4Cl and refluxed at 60 °C to 80 °C for 3 h. The NH_4Cl treated zeolite was separated by filtration, washed with water, and followed by two more repetitions of the ion-exchange process. Finally, the ammonium-type zeolite material was dried and then calcined at 550 °C to get H-type zeolites. The inductively coupled plasma (ICP) analyses of the digested sample showed a complete removal of the counter cations by repeated treatments with NH_4Cl solutions.

The catalytic methanol dehydration efficiency of the zeolite materials was compared with three different samples of the industrial catalyst, γ-Al_2O_3. In addition to a commercial γ-Al_2O_3 (Nippon Aerosil, Japan), and a reference γ-Al_2O_3 JRC-ALO-6 obtained from the Catalysis Society of Japan, yet another sample of γ-Al_2O_3 was prepared in our laboratory from a stepwise calcination of boehmite (Wako, Japan) precursor. An appropriate amount of boehmite was taken in a ceramic crucible and calcined at 600 °C for 2 h. At the end of the reaction, the crucible was quenched in air. The obtained product was homogenized by grinding and then re-calcined in a ceramic crucible at 700 °C for 14 h and quenched in air. Thus obtained final product was ground well and used for characterization and in catalytic methanol dehydration testing.

2.2. Characterization

Powder XRD patterns were recorded on Rigaku UltimaIII diffractometer using Cu Kα at 40 kV and 40 mA. The XRD patterns were recorded in the 2-theta range of 5° to 50° for the zeolites and 20° to 80° for the γ-Al_2O_3 samples at a scanning speed of 0.01° min^{-1}. Field-emission SEM images were taken on Hitachi S-5200 microscope operated at 2 kV. The chemical composition of the digested zeolites was examined by ICP analysis, using Shimadzu ICPE-9000 spectrometer. For the ICP analysis, at first, the solid zeolite samples were digested in 4 M KOH (Wako, Japan) aqueous solution to prepare a clear solution. N_2 adsorption-desorption isotherms

were measured on Belsorp-miniII (BEL, Japan) apparatus at liquid N_2 temperature. Before recording the N_2 sorption isotherms, the samples were outgassed for 6 h at 150 °C. Specific surface area and micropore volume were calculated by BET and the appropriately applicable t-plot methods (for the microporous material), respectively. Temperature programmed desorption (TPD) profiles for NH_3 desorption were assessed on Multitrack TPD instrument of BEL, Japan. Vibrational spectra were recorded on JASCO Fourier transformed infrared (FT-IR) spectrometer, model 7300 (Jasco, Japan). A thin disk of 20 mm diameter was prepared from about 30 mg of the zeolite powder for the *in-situ* methanol sorption studies by FT-IR spectroscopy. A self-sustaining disk of the catalyst was placed in a home-made quartz cell with a NaCl window and pre-treated at 500 °C for 1 h under evacuation. Then the temperature was lowered down to RT and gas-phase methanol (0.5 kPa) with H_2O was introduced into the cell and treated at various temperatures. Thermogravimetric-differential thermal analysis (TG-DTA) profiles of the spent zeolites and γ-Al_2O_3 catalysts were recorded on Rigaku Thermo Plus apparatus (Rigaku, Japan).

2.3. Catalytic activity test

All the various small-pore zeolites and the γ-Al_2O_3 samples were tested for the methanol dehydration under different reaction conditions. A schematic of the setup for the catalytic dehydration of methanol is provided in Fig. S1. The gas-phase methanol conversion reaction was carried out in a fixed-bed reactor. Typically, 0.1 g of the H-type zeolite catalyst or γ-Al_2O_3 material was sandwiched between quartz wool and packed in a quartz tube reactor housed in a furnace (Fig. S1). The reactor was equipped with a well-calibrated online Shimadzu gas chromatograph (GC) GC–14B where hydrocarbons were separated in an HP-PLOT Q column and analyzed by a flame ionization detector (FID). In methanol dehydration reaction, 5 kPa–20 kPa of gas-phase methanol (99.8%, Wako, Japan) was steadily flown over the catalyst bed at a temperature range of 150 °C to 200 °C. Liquid-phase methanol was fed by a flow-controlled syringe pump to an evaporator where it was mixed with helium before its gas-phase injection to the catalytic reactor. Prior to the introduction of methanol, a pre-treatment of the catalyst packed in the tube reactor was carried out at 500 °C for 1 h. Afterward, the reactor was adjusted to the required temperature for studying the methanol dehydration reaction. Kinetic parameters like weight/flow (W/F) rate and weight hourly space velocity (WHSV) were varied from 34 g h mol^{-1} to 8 g h mol^{-1} and 1.0 h^{-1} to 3.8 h^{-1}, respectively.

The very first analysis of the gaseous products at the outlet was performed after 10 min of the start of the reaction. Later on, the reaction products were analyzed every 30 min during the steady-state reaction conditions. Methanol conversion was defined as the mass of the consumed methanol divided by the mass of the methanol fed into the reactor. Selectivity to the reaction product(s) was calculated on the carbon mass basis of the effluent gas from the tube reactor detected by on-line GC-FID and the values are expressed as carbon percent. Under the same reaction conditions, the methanol dehydration efficiencies of the zeolites were compared with three samples of γ-Al_2O_3; commercial γ-Al_2O_3, reference γ-Al_2O_3 JRC-ALO-6 obtained from the Catalysis Society of Japan, and a laboratory-synthesized γ-Al_2O_3.

3. Results and discussion

3.1. Physicochemical properties of the catalyst materials

XRD pattern of the as-prepared Rho showed that the synthesized material is a highly crystalline, phase-pure RHO-type zeolite
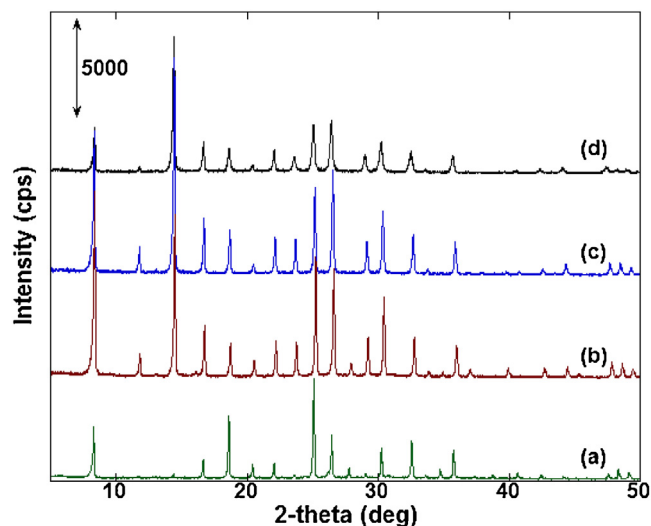

Fig. 1. XRD patterns of Rho zeolite; as-prepared (a), ammonium-type (b), H-type (c), and the spent Rho zeolite after catalytic methanol dehydration reaction (d).
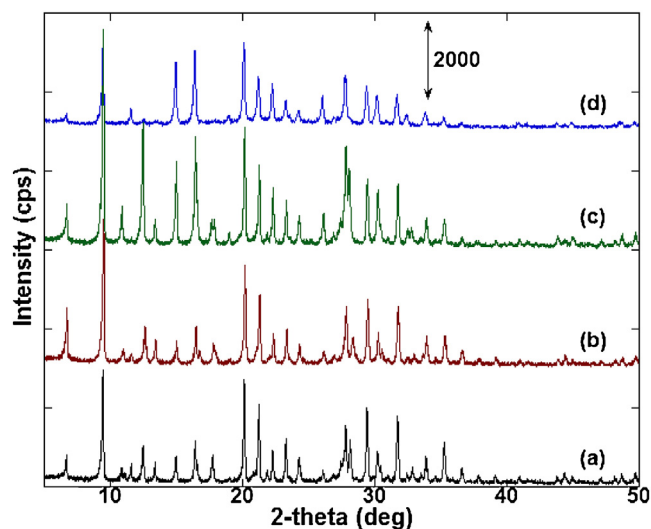

Fig. 2. XRD patterns of KFI zeolite; as-prepared zeolite containing structure directing agent (SDA; a), calcined at 550 °C for removal of organic SDA (b), ammonium-type (c), and the spent KFI zeolite after catalytic methanol dehydration reaction (d).

(Fig. 1a). The typical crystalline nature of the RHO-type topology was maintained after the exchange of cesium ions with ammonium ions (Fig. 1b) and its subsequent conversion to H-type zeolite (Fig. 1c). As estimated by ICP analysis, counter cations are completely removed by ammonium exchange reaction and the Si/Al ratio of H-Rho is 3.5, which is lower than the Si/Al ratio of the starting composition of the synthesis gel (5.0). It is important to note from a practical viewpoint, that the zeolite Rho is synthesized in the absence of any organic SDA. For a majority of the synthetic zeolites, organic SDA is the most costly reagent. In addition to the economic advantage, organic SDA-free synthesis is environmentally friendly. Imitating the natural settings for the formation of zeolites, organic SDA-free syntheses of zeolites are getting much attention in making them environmentally benign and industrially more practicable [15,16]. XRD pattern of the as-made KFI demonstrated that the topology of the obtained material belongs to KFI-type (Fig. 2a). Essentially, all the diffraction peaks correspond to the KFI-type topology of the zeolite, hence showing a high crystalline phase-purity of the product. The zeolite material basically maintained its

Table 1
Physicochemical properties of various zeolites and γ-Al$_2$O$_3$ catalysts.

Catalyst	Si/Al ratio[a] Product(Gel)	S_{BET}[b] (m^2 g^{-1})	V$_{micropore}$[b] (cm^3 g^{-1})	Amount of acid sites[c] (mmol g^{-1})		Size[d] (μm)
				'l' peak	'h' peak	
Rho	3.5(5.0)	812	0.429	1.173	1.361	1
KFI	3.3(5.0)	382	0.203	0.841	0.814	12
Commercial ZSM-5	23.3	348	–	0.727	0.729	–
Commercial γ-Al$_2$O$_3$	–	112	–	0.074	0.272	–
Lab-prepared γ-Al$_2$O$_3$	–	176	–	0.113	0.412	–
γ-Al$_2$O$_3$ JRC-ALO-6	–	177	–	0.086	0.386	–

[a] From ICP analysis.
[b] Determined from N$_2$ adsorption-desorption isotherms.
[c] Estimated from the NH$_3$-TPD profiles.
[d] Average size of the crystallites was estimated from SEM images.

KFI-type topology after heat treatment, for removal of the organic SDA (Fig. 2b), and further upon the exchange of the cations with ammonium ions (Fig. 2c). ICP analysis confirmed on the removal of K and Sr cations from the KFI structure by the ammonium ion-exchange process. The Si/Al ratio of 3.3 for the H-KFI was lower than the starting composition of the synthesis gel (5.0). The physicochemical properties of the KFI and Rho zeolites are summarized in Table 1.

As shown in Fig. 3A, SEM image further confirmed the crystalline nature of the product and revealed a typical polyhedral sphere-like morphology for the zeolite Rho. The average size of the crystallites of Rho zeolite is around 1 μm. ICP analysis showed a small increase (7–10%) in the Si/Al ratio for the Rho zeolite samples obtained from the synthesis gel with Si/Al ratios of 10 and 20. The size of the Rho crystallite also slightly increased with an increase in the Si/Al ratio of the synthesis gel along with a sharpening of the facets of the polyhedral spherical particles (Fig. S2). XRD studies showed that crystalline phase-pure Rho is obtained from all the synthesis gels with different Si/Al ratios from 5 to 20 (Fig. S2). Importantly, the crystalline nature and morphology of the RHO-type zeolite are preserved after its chemical treatments in changing from alkali metal type to H-type solid-acid catalyst. SEM images confirmed the well-formed crystalline nature of the as-prepared KFI zeolite too and revealed the presence of typical aggregates of cube-like particles

of about 12 μm (Fig. 3C), much larger than the crystallite size of Rho zeolite (1 μm). The crystalline nature was maintained upon chemical treatments of the as-prepared KFI to form H-type KFI. However, its surface showed some deterioration upon ammonium ion exchange reaction. In contrast, Rho zeolite demonstrated a higher chemical stability upon ammonium ion-exchange reaction.

N$_2$ adsorption-desorption isotherms for H-Rho are also typical that of the microporous materials (Fig. 4Ab). As noted in Table 1, H-Rho demonstrated a relatively high specific surface area (S_{BET}, 812 m^2 g^{-1}) and micropore volume (0.429 cm^3 g^{-1}) in comparison with H-KFI, and other typical zeolitic materials widely employed for the methanol valorization processes e. g. ZSM-5 (Table 1). Fig. 4Aa shows N$_2$ adsorption-desorption isotherms for H-KFI that are also typical of the microporous materials. As calculated by the BET equation, H-KFI showed a moderate specific surface area of 382 m^2 g^{-1}. The micropore volume of 0.203 cm^3 g^{-1} calculated by the appropriately employed t-plot method also demonstrated a medium level of porosity for the H-KFI zeolite. The micropore volume and S_{BET} of H-KFI are comparable with a wide range of the values reported for the most investigated SAPO-34 and ZSM-5 catalysts but lower than the zeolite Rho (Table 1).

NH$_3$-TPD profile for H-Rho showed two prominent 'l' and 'h' peaks around 210 °C and 530 °C, respectively (Fig. 4Bb) [16]. The desorption temperature region for 'l' peak is typical for weak acid
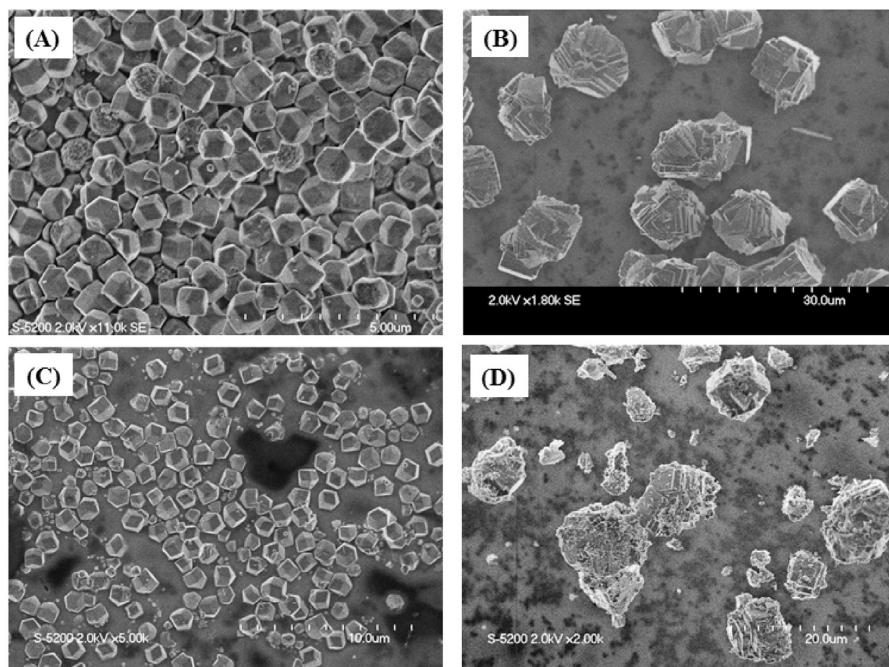

Fig. 3. SEM images of as-prepared zeolite Rho (A), KFI (B), and spent zeolite catalysts after methanol conversion reaction over Rho (C) and KFI (D).
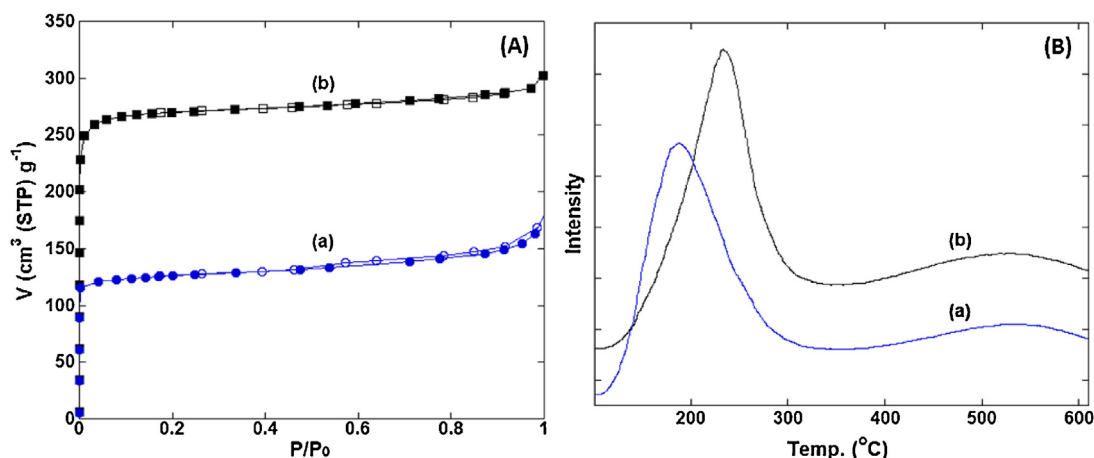
Fig. 4. N_2 adsorption-desorption isotherms (A), and temperature programmed desorption profiles for NH_3 (B) for the H-type zeolite catalysts KFI (a), and Rho (b).

sites, and that of '*h*' peak with a long shoulder on the lower side is for medium-strong acid sites. The total concentration of the solid-acid sites on H-Rho (2.53 mmol g^{-1}) is larger than that on the H-KFI (1.65 mmol g^{-1}) but smaller than the theoretical value for the Si/Al ratio of 3.5. For both the zeolites, the TPD '*h*' peaks for NH_3 appeared around similar temperatures, indicating a comparable strength of their strong solid-acid sites (Fig. 4B). In contrast to a low concentration of medium-strong acid sites on H-KFI, the concentration of medium-strong acid sites is high for the H-Rho zeolite (Fig. 4B). NH_3-TPD profile for H-KFI showed two peaks for desorption of NH_3 (Fig. 4Ba). The '*l*' and '*h*' peaks appeared around 190 °C and 530 °C, respectively, demonstrating the presence of both weak and medium-strong solid-acid sites. The intensity of the TPD '*l*' peak for NH_3 is much pronounced than that of the '*h*' peak, indicating a high concentration of the weak solid-acid sites. The total concentration of solid-acid sites on H-KFI (1.65 mmol g^{-1}) is comparatively lower than the value predicted from the Si/Al ratio of 3.3.

The calcination of boehmite produced γ-Al_2O_3, as shown by the XRD pattern (Fig. S3A). The crystalline nature of the γ-Al_2O_3 prepared by two-step calcination is closer to that of the reference γ-Al_2O_3 JRC-ALO-6. The measured BET specific surface area for the commercial γ-Al_2O_3 is 112 $m^2 g^{-1}$. In comparison with the commercial γ-Al_2O_3, both the other γ-Al_2O_3 samples showed about 1.6 times higher S_{BET}, ~177 $m^2 g^{-1}$ (Table 1). NH_3-TPD profile for the laboratory-synthesized γ-Al_2O_3 is closer to that of the reference γ-Al_2O_3 JRC-ALO-6 (Fig. S3B). Both these γ-Al_2O_3 materials depicted two prominent '*l*' and '*h*' peaks with a similar level of weak acid sites. And '*h*' peak of the reference JRC-ALO-6 material showed the relatively strongest level of medium acidic sites among all the γ-Al_2O_3 samples. On the contrast, the '*h*' peak intensity and level of acidic strength for the commercial γ-Al_2O_3 sample are at the lowest level in the γ-Al_2O_3 materials, and the calculated values are reported in Table 1. In comparison with the temperature range for the medium-strong acidity of zeolite Rho and KIF, the temperature for the '*h*' peak top of γ-Al_2O_3 samples is lying at a relatively lower level, in the medium acidity range.

3.2. Methanol dehydration to DME

Results from 5 kPa feed of methanol at WHSV of unity for 24 h time-on-stream (ToS) methanol dehydration reactions over Rho zeolite at temperatures from 150 °C to 200 °C are demonstrated in Fig. 5A. At 200 °C, a thermodynamically limited (~93%) level of methanol dehydration with 100% selectivity to DME is demonstrated by Rho zeolite. All the catalytic testing results presented here are for the Rho zeolite synthesized from the gel with Si/Al

ratio of 5. Similar results are obtained for the methanol conversion efficiencies over Rho zeolite samples synthesized from initial Si/Al ratios of 10 and 20. At the beginning of methanol dehydration reaction (< 30 min), a spike in the conversion efficiency may come from the physical sorption of methanol (Figs. 5A, & 6A). A small decrease in the methanol conversion efficiency (~2%) is observed when the dehydration reaction is carried out at 180 °C. For both these reaction conditions (180 °C and 200 °C), DME is the only product with an overall mass balance of 100%. Upon further lowering the dehydration reaction temperature down to 150 °C, more than 70% methanol conversion with a complete selectivity to DME is recorded over Rho zeolite (Fig. 5A). Under the same dehydration reaction conditions (200 °C), the best performing reference material, γ-Al_2O_3 JRC-ALO-6 showed less than 80% methanol conversion efficiency (Fig. 5B). Interestingly, the lowest catalytic efficiency of the Rho zeolite (at 150 °C) is comparable with the highest efficiency recorded for the best-performing γ-Al_2O_3. And for the dehydration reaction at 180 °C, the catalytic efficiency of the reference γ-Al_2O_3 did not exceed over 50%. For the dehydration reaction at 150 °C, Rho zeolite demonstrated a 10 times enhancement over the most active reference γ-Al_2O_3 material (Fig. 5). For a long term stability check of Rho zeolite, methanol dehydration at 180 °C and 200 °C was continuously run for about 3 days. Importantly, Rho zeolite demonstrated a stable performance in the long runs without losing any activity and complete selectivity to DME.

At the optimized methanol dehydration reaction temperature (200 °C for γ-Al_2O_3), WHSV values were varied at 1.0 h^{-1}, 2.4 h^{-1} and 3.8 h^{-1} corresponding to 5 kPa, 10 kPa and 20 kPa of methanol, respectively. A thermodynamically limited (~93%) methanol dehydration is maintained for 24 h over Rho zeolite at all the various reaction conditions of WHSV (Fig. 6). The highest methanol conversion (at 5 kPa) over the reference γ-Al_2O_3 (78%) is about 14% less than the efficiency of the Rho zeolite (Fig. 6A). Under the same optimized reaction conditions, the commercial γ-Al_2O_3 showed merely 47% conversion of methanol. Regarding the product selectivity, DME is the main product over reference γ-Al_2O_3 samples, although traces of C_1–C_3 hydrocarbons are also noticed. Other studies have also reported a similar behavior towards methanol conversion product selectivity over γ-Al_2O_3 samples. Importantly, for the methanol conversion reactions over Rho zeolite, DME is the only product and no other products are detected in the effluent gas for the reaction carried out at or below 200 °C.

As shown in Fig. 6B, the catalytic dehydration efficiency of Rho zeolite for the methanol feed pressure of 10 kPa is maintained at ~93%. On the contrary, methanol dehydration efficiency of the reference γ-Al_2O_3 JRC-ALO-6 decreased to about 47%. The gap
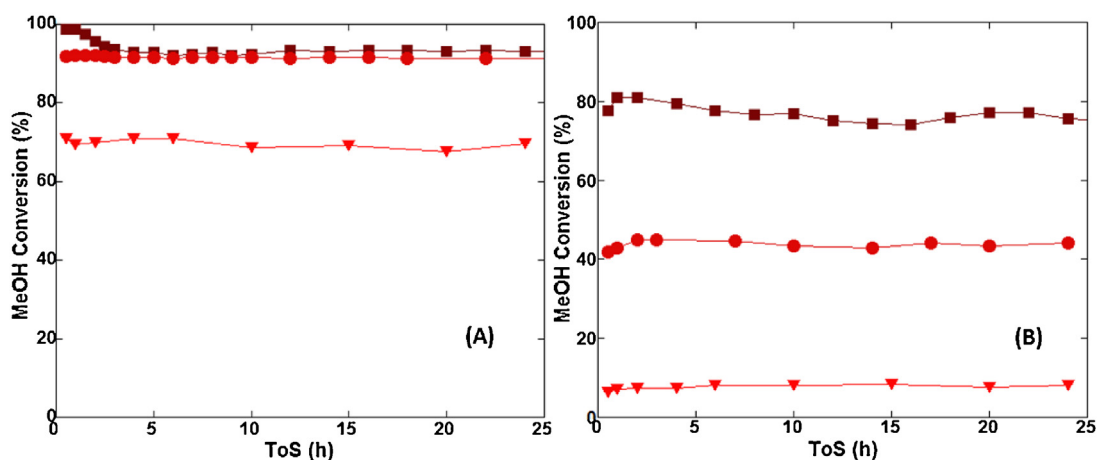
Fig. 5. Methanol conversions over zeolite Rho (A), and reference γ-Al$_2$O$_3$ JRC-ALO-6 (B) at various reaction temperature conditions 150 °C (▼), 180 °C (●), and 200 °C (■) at WHSV values 1.0 h^{-1}.
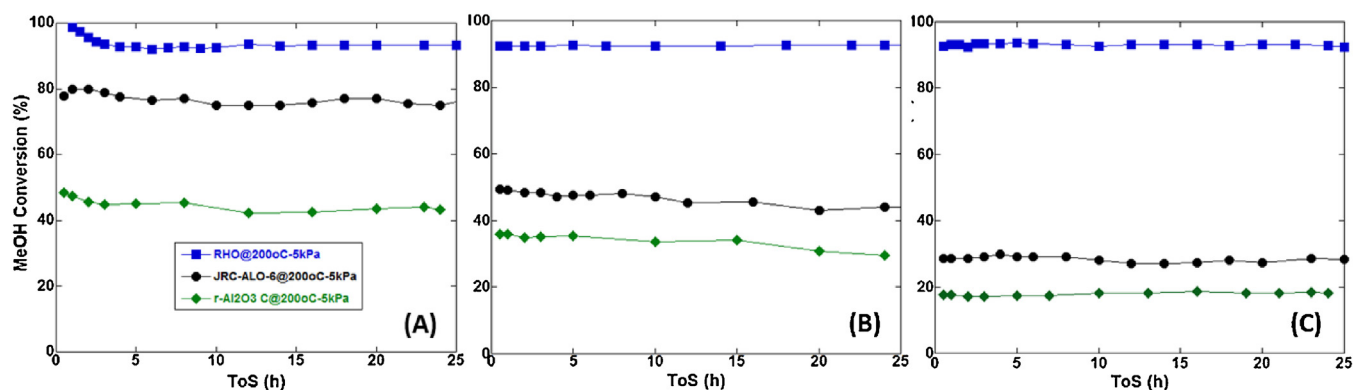

Fig. 6. Methanol conversions over zeolite Rho (■), reference γ-Al$_2$O$_3$ JRC-ALO-6 (●), and commercial γ-Al$_2$O$_3$ (♦) at 200 °C, and different WHSV values 1.0 h^{-1} (A), 2.4 h^{-1} (B), and 3.8 h^{-1} (C).

between the efficiency of Rho zeolite and the reference γ-Al$_2$O$_3$ JRC-ALO-6 increased from 14% (for 5 kPa) to 50% (for 10 kPa). The catalytic methanol dehydration efficiency of the commercial γ-Al$_2$O$_3$ showed a further decrease from 47% (for 5 kPa) to 37% (for 10 kPa). From a practical viewpoint, it is critical to note that for the methanol feed pressure of 20 kPa with WHSV 3.8 h^{-1} a further decrease in the methanol conversion efficiency is observed over the reference γ-Al$_2$O$_3$ JRC-ALO-6 and the commercial γ-Al$_2$O$_3$ (Fig. 6C). On the contrast, the Rho zeolite maintained its methanol dehydration efficiency to DME under the increased pressure of methanol feed (20 kPa) demonstrating a good prospect for the application of this catalyst.

Catalytic methanol conversion efficiencies of different zeolites with 2-D and 3-D channels and three different γ-Al$_2$O$_3$ samples are illustrated in Fig. 7. All the reaction parameters were kept constant and methanol dehydration reaction was carried out at 200 °C. In comparison with the γ-Al$_2$O$_3$ samples, all the investigated 3-D zeolites, Rho, KFI, and SSZ-13 exhibited a thermodynamic level of methanol conversion with a 100% selectivity to DME. The CHA-type zeolite SSZ-13 (Si/Al 14), an aluminosilicate homolog of SAPO-34 is synthesized with a very high S_{BET} (1104 m^2 g^{-1}) [14]. Another small-pore zeolite, Linde W with a 3-D framework showed a moderate methanol dehydration efficiency and at relatively high temperature (325 °C), pertaining to its intrinsically mild solid-acid properties, [7]. So, an appropriate extent and strength of solid-acid sites are found important for a low-temperature dehydration of methanol to DME. Next, the zeolite RUB-13 with the 2-D framework and a medium level of acidity is found less active for methanol
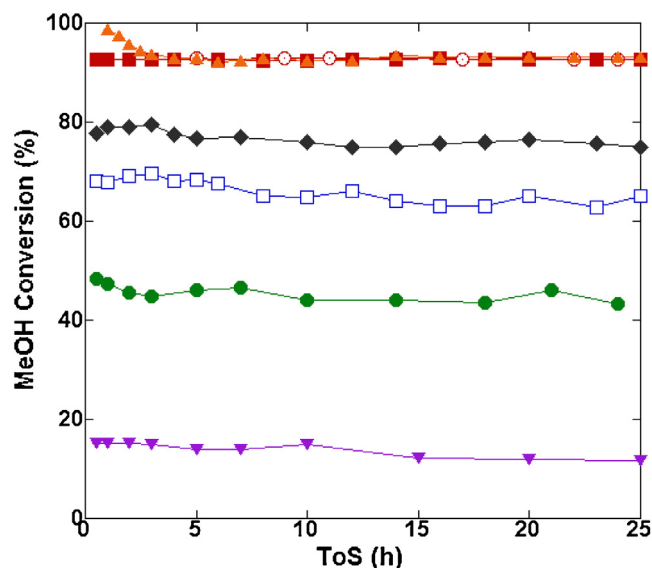

Fig. 7. Methanol conversions at 200 °C and WHSV 1.0 h^{-1} over various zeolites; Rho (▲), KFI (■), SSZ-13 (○), RUB-13 (▼), and commercial γ-Al$_2$O$_3$ (●).

dehydration at 200 °C. Besides this low-temperature inactivation of methanol on the medium level acidity of RUB-13, the accessibility of methanol to the active sites is rather low in the 2-D porous structures. Therefore, a 3-D porous structure with a suitably opti-

mum strength and extent of solid-acid sites is found as optimized material for the dehydration reaction.

In addition to the various physicochemical properties e. g. specific surface area and particle size of the catalysts, the strength of medium-strong solid-acid sites represented by the position of the 'h' peak in the NH$_3$-TPD profiles is found important for the catalytic dehydration activity. NH$_3$-TPD profiles of the three γ-Al$_2$O$_3$ samples are presented in Fig. S3B. All the samples showed two prominent peaks, namely 'l' and 'h' originating from the desorption of NH$_3$ at low and high temperature, respectively. The peak tops of the 'l' peaks for the γ-Al$_2$O$_3$ samples appeared around similar temperature. However, the peak top of the 'h' peak, corresponding to the medium-strong level of acid sites, for the commercial γ-Al$_2$O$_3$ appeared at the lowest temperature (305 °C) followed by the position for the γ-Al$_2$O$_3$ prepared from the calcination of boehmite (325 °C). Among all the γ-Al$_2$O$_3$ samples, JRC-ALO-6 reference material demonstrated the highest strength of the acidic sites with the TPD 'h' peak top for NH$_3$ at 352 °C. The concentrations of solid-acid sites on γ-Al$_2$O$_3$ samples are reported in Table 1.

Methanol dehydration efficiency was correlated with the solid-acid strength of all the different γ-Al$_2$O$_3$ catalyst materials. Over the γ-Al$_2$O$_3$ samples, conversion of diluted methanol linearly increased with an increase in the strength of the acidic sites (Fig. S4). From the extrapolation of the straight line (R 0.99) for the γ-Al$_2$O$_3$ samples, a threshold 'h' peak temperature value of about 370 °C corresponding the medium-strong level of acidity is calculated for a thermodynamically leveled conversion of methanol. Sung et al. correlated the acidity determined by FT-IR with the methanol dehydration catalytic activity of different crystalline phases of aluminum oxide [20]. Here in this study, we have compared the methanol dehydration over different samples of γ-Al$_2$O$_3$ crystalline phase against the acidity determined by NH$_3$-TPD. Crystalline phase purity of aluminum oxide and appropriate mixing are important factors in controlling their efficiency for the methanol dehydration reaction. As shown in Fig. 4B, the 3-D zeolites possess a high concentration of medium-strong acidic sites with the 'h' peak temperatures well above the threshold, 370 °C (Table 1). Due to the thermodynamic restrictions, however, methanol conversions are leveled off around 93%. The ratio of weak and medium acidity of beta type zeolite was modulated by loading different amounts of Ca in controlling its methanol dehydration efficiency [9]. Migliori et al. examined MFI-type zeolites with different Si/Al ratio and a higher acidity was found favorable for methanol dehydration reaction [21]. Essentially, it is found that methanol activation energy increased against the solid-acidic properties of the γ-Al$_2$O$_3$ catalysts (Fig. S4). Hence, ours this study confirms on low-temperature activation of methanol dehydration reaction over Rho and KFI zeolites with an appropriately higher strength and the amount of medium-strong acidity (Fig. 4B). Under the same reaction conditions, catalytic dehydration efficiency of ZSM-5 and SSZ-13 with suitable solid-acid properties further confirms this finding (Figs. 7 & S5). However, ZSM-5 has challenges of product selectivity and loss of activity due to coke deposition. Formation of other hydrocarbons over ZSM-5 was observed at 225 °C [12]. NH$_3$-TPD 'h' peak temperature for the 2-D zeolite, RUB-13 is also in the range of medium acidity around 380 °C [15]. However, methanol conversion over the 2-D zeolites is rather low, probably due to limited diffusion (Fig. 7). At a specific reaction temperature, the concentration of accessible acid sites is important in determining the efficiency of the methanol dehydration catalyst. For DME synthesis in the temperature range of 180 °C to 300 °C, the zeolite FER with a 2-D framework was found efficient than the 3-D BEA and MFI type zeolites when the reaction was carried out at a higher temperature [22]. Similarly, zeolite RUB-13 has prospects of efficient methanol dehydration at a temperature relatively higher than the working conditions of Rho, KFI, and SSZ-13. But, at high-temperature, the reaction product selectively shift

towards hydrocarbons [14–16], and in this study, we are focusing on a low-temperature catalytic dehydration of methanol to DME. Wei et al. reported that besides optimized acidity of ZSM-5, an increased diffusion capability was an important factor in enhancing its activity for methanol dehydration to DME [23]. So, a 3-D porous structure with medium-strong solid-acid sites may be important for a low-temperature dehydration of methanol, and other alcohols too.

In comparison with the reported studies, the catalytic dehydration performance of the investigated small-pore 3-D zeolites Rho, KFI, and SSZ-13 is similar with that of the ZSM-5 and superior to the other zeolitic materials and γ-Al$_2$O$_3$ samples. Extended run for methanol dehydration reaction over zeolite Rho was performed for 3 days, and it exhibited a constant performance with no appreciable loss observed in the activity and selectivity towards DME. A commercial ZSM-5 (Si/Al 23.3) sample with a moderately high S_{BET} (348 m^2 g^{-1}) and comparable solid-acid properties (Table 1) was also employed for methanol dehydration reaction at 200 °C, and WHSV 3.8^{-1}. As shown in Fig. S5, both Rho and ZSM-5 depicted similar, thermodynamically limited efficiencies ($\sim$93%). On the other hand, two samples of γ-Al$_2$O$_3$, an industrial catalyst for methanol dehydration showed less than 30% efficiency. Mostly, methanol dehydration activities of the reported materials were studied at temperatures higher than 200 °C, where the formation of hydrocarbons is inevitable and so was observed on ZSM-5. Fu et al. reported ZSM-5 and Y (3-D structure) for methanol conversions of about 90% and 70% respectively, at 200 °C [13]. Stability of the framework structure may affect the performance of a particular zeolite; even when Linde W was activated in a stream of pure helium, methanol conversion thereupon was not more than 40%, at 325 °C [7]. Baek et al. reported clinoptilolite (methanol conversion of 97%), SAPO-34 (91%), and ferrierite (91%) for methanol dehydration at 250 °C [24]. In the NH$_3$-TPD profiles, the 'h' peak temperature of SAPO-34 was 415 °C, and for the other two zeolites, it has shifted towards high temperature. However, the reported methanol conversion over clinoptilolite was beyond thermodynamic limit. DME selectivity over SAPO-34 was rather low (86%) and furthermore, it deactivated quickly. Although employed at a relatively higher reaction temperature (250 °C), the dehydration activity of SAPO-34 (3-D structure) and ferrierite (2-D structure) was lower than that of Rho, KFI, and SSZ-13 zeolites examined in this study (Fig. 7).

After the dehydration reactions, the spent catalysts Rho and KFI were investigated by XRD, SEM and TG-DTA techniques. The spent Rho catalyst showed a high stability with regards to its crystalline structure and morphology, though spent KFI showed moderate changes in the physicochemical properties. Essentially all the main diffraction peaks appeared in the XRD patterns of the spent Rho zeolite (Fig. 1d) and KFI (Fig. 2d), and demonstrated a high crystalline stability of the zeolites. SEM photos of spent Rho and KFI are shown in Fig. 3. Morphology and crystallite size of Rho zeolite remained unchanged after methanol dehydration reaction (Fig. 3C). On the other hand, KFI zeolite showed some deformation of morphology and aggregation but kept its crystalline nature (Fig. 3D). SEM images showed a deterioration of KFI morphology during the preparation of its H-type material by the ammonium exchange process. Similar results on the high stability of crystalline structure and morphology of the Rho zeolite are observed for the MTO reactions carried out at higher temperatures ($\geq$350 °C) too [16].

TG-DTA profiles of the spent Rho, ZSM-5, and γ-Al$_2$O$_3$ samples are depicted in Fig. S6. In comparison with the zeolites, both the γ-Al$_2$O$_3$ samples showed a minor (<3%) weight loss for heating up to 400 °C indicating a small amount of methanol adsorbed on them. ZSM-5 showed a significant weight loss (>7%) while the highest weight loss ($\sim$17%) was observed for the spent Rho zeolite. The corresponding DTA profile illustrated exothermic nature of the weight loss reaction from the methanol-derived organic species. These TG-
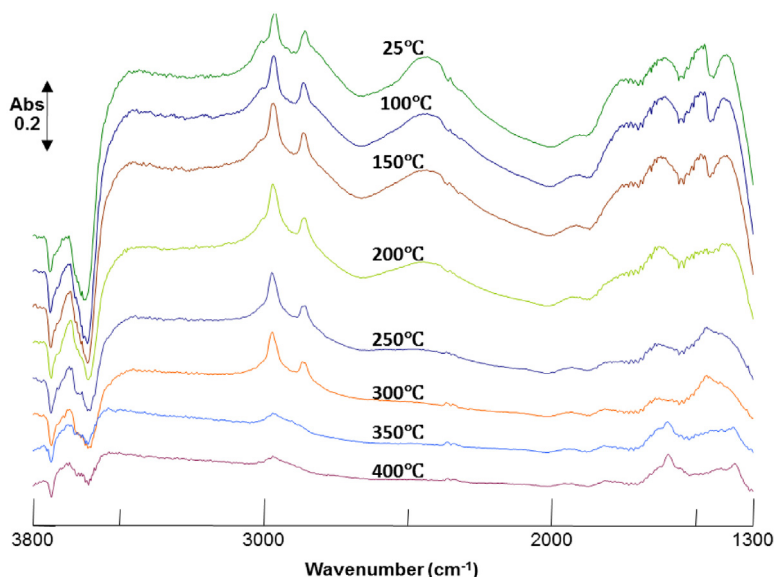
Fig. 8. *In-situ* FT-IR spectra of methanol sorption on zeolite Rho at various temperatures.

DTA profiles demonstrate on the availability of the largest number of active site on Rho followed by ZSM-5. TG-DTA comparison of commercial γ-Al$_2$O$_3$ and the reference γ-Al$_2$O$_3$ JRC-ALO-6 showed an enhanced methanol sorption on the later and so is the methanol dehydration efficiency.

From a practical viewpoint, the methanol dehydration studies carried out with a high concentration (20 kPa) of methanol are interesting for an extended reaction time. The W/F and WHSV were kept at 8 g cat. h mol^{-1} and 3.8 h^{-1}, respectively. The results of 24 h-on-stream dehydration reaction are depicted in Fig. 6C. In comparison with the stable dehydration reaction at low methanol pressure, the conversion efficiency over γ-Al$_2$O$_3$ catalysts decreased. However, zeolite Rho maintained its remarkable activity under both low and high pressures of methanol feed. Commercial γ-Al$_2$O$_3$ showed the lowest conversion (17%) followed by JRC-ALO-6 reference material (29%). At all the reaction conditions, 5 kPa–20 kPa of methanol, the efficiency of JRC-ALO-6 reference material is always higher than the efficiency of the commercial γ-Al$_2$O$_3$. The dehydration efficiencies of γ-Al$_2$O$_3$ samples are sequentially decreasing on going from 5 kPa to 10 kPa of methanol and further lowering down with 20 kPa of methanol. Interestingly, the methanol conversion efficiency of Rho (and KFI too) remained at the thermodynamically limited level, illustrating a good prospect of 3-D small-pore zeolite for an application in the commercial production of DME. The best zeolite material reported for methanol dehydration, ZSM-5 is used as a control catalyst. As shown in Fig. S5, a similar level of methanol conversion was observed over Rho and ZSM-5. In comparison with KFI, Rho zeolite showed a better stability under methanol conversion reaction as shown in SEM images (Fig. 3). A faster deactivation of KFI compared with that of Rho is observed in the methanol conversion to olefins at a lower reaction temperature (350 °C). The strength of solid-acid sites is at a comparable level for both of these zeolites giving a thermodynamic conversion of methanol, while the longer life and stability of Rho could be attributed to its high amount of medium-strong acid sites (Table 1). In comparison with relatively larger particles of KFI, a smaller crystallite size of Rho and its high specific surface area (Fig. 3, Table 1) may also play an important role in its enhanced catalytic lifetime.

In-situ FT-IR investigations were carried out in a home-made cell to understand methanol sorption on Rho zeolite and its significance in the valorization process. FT-IR spectrum of Rho zeolite

recorded at RT after pre-treatment (at 500 °C) is shown in Fig. S7. A difference of the two spectra obtained by subtracting the bare zeolite spectrum from that of the methanol adsorbed zeolite spectrum depicted negative bands for [Si—OH] and [Si—OH—Al] vibrations. This observation of negative bands illustrated the consumption of hydroxyl groups upon the sorption of methanol species [14]. Furthermore, two positive and strong bands appeared at 2973 cm^{-1} and 2864 cm^{-1} corresponding to the —CH stretching vibrations from the adsorbed methoxy species. Next, the temperature of the IR cell was raised from RT to 400 °C and step-by-step changes with the IR absorbance are depicted in the differential spectra (Fig. 8). Essentially, the methoxy species remained strongly adsorbed on the surface of Rho zeolite for the temperature range of 25 °C to 300 °C. The IR absorbance intensity started to decrease from 200 °C onward. And a complimentary restoration of the structural hydroxyl group of the zeolite is seen with methanol desorption. A similar behavior of methanol adsorption and desorption on CHA-type SSZ-13 was reported by Zhu et al. [14]. Pertaining to this low dehydration reaction temperature (200 °C), the TG-DTA profile of the spent Rho demonstrated a significant weight loss from desorption of methanol species (Fig. S6). A significant decrease in the —CH stretches is observed for the thermal treatments beyond 300 °C complimenting the evidence from TG-DTA studies. Initial (<100 °C) weight loss for the spent Rho zeolite may come from the physical sorption of methanol as it is seen at the beginning of the dehydration reaction. Adsorption and desorption of water are monitored from the IR absorption for —OH of water at 1630 cm^{-1}. For the temperatures $\geq$ 200 °C IR spectra for water demonstrated less absorption and indicated a persistently high activity. The absence of IR absorbance band for the hydroxyl group associated with the extra-framework Al (ca. 3660 cm^{-1}) demonstrated a good stability of the Rho zeolite catalyst under working conditions, and supported the findings of XRD and SEM studies.

4. Conclusions

Small-pore zeolites Rho, KFI and SSZ-13 with medium-strong acidic properties demonstrated a thermodynamically limited methanol conversion ($\sim$93%) efficiency at low temperatures ($\leq$200 °C). Product selectivity over the small-pore 3-D zeolites remained 100% to DME. The catalytic methanol dehydration performance of these small-pore zeolites is similar to that of the ZSM-5

which is prone to coke deposition and co-formation of higher hydrocarbons. Furthermore, methanol dehydration over the small-pore zeolites is far better than the three different samples of the industrial catalyst, γ-Al$_2$O$_3$. Another small-pore zeolite, RUB-13 with a 2-D structure and a medium level of solid-acid properties is less effective in methanol dehydration at low-temperature. In conclusion, pertaining to their stable 3-D porous structures and appropriate medium-strong solid-acid properties, selective dehydration of methanol into DME with a maximum efficiency makes Rho, KFI, and SSZ-13 zeolites attractive candidates for practical applications. Among the most active small-pore zeolites, the zeolite Rho is on the top probably due to its extremely high specific surface area (812 m^2 g^{-1}) and smaller crystallite size (1 μm), and consequently, it demonstrated a stable performance in 3 days long-run of the dehydration reaction. Especially, a remarkable stable performance of this Rho zeolite synthesized without any organic structure directing agent offers a good prospect for its application to methanol valorization process for the production of greener synthetic fuel, DME.

Acknowledgements

Appendix A. Supplementary data

Supplementary data associated with this article can be found, in the online version, at http://dx.doi.org/10.1016/j.apcatb.2017.05.089.

References

[1] J. Sun, G. Yang, Y. Yoneyama, N. Tsubaki, Catalysis chemistry of dimethyl ether synthesis, ACS Catal. 4 (2014) 3346–3356.
[2] T.A. Semelsberger, R.L. Borup, H.L. Greene, Dimethyl ether (DME) as an alternative fuel, J. Power Sources 156 (2006) 497–511.
[3] J.J. Spivey, Review: dehydration catalysts for the methanol/dimethyl ether reaction, Chem. Eng. Commun. 110 (1991) 123–142.
[4] M. Stöcker, Methanol-to-hydrocarbons: catalytic materials and their behavior, Microporous Mesoporous Mat. 29 (1999) 3–48.
[5] C.D. Chang, Hydrocarbons from methanol, Catal. Rev. 25 (1983) 1–118.
[6] F. Yaripour, F. Baghaei, I. Schmidt, J. Perregaard, Catalytic dehydration of methanol to dimethyl ether (DME) over solid-acid catalysts, Catal. Commun. 6 (2005) 147–152.
[7] Y.-H. Seo, E.A. Prasetyanto, N. Jiang, S.-M. Oh, S.-E. Park, Catalytic dehydration of methanol over synthetic zeolite W, Microporous Mesoporous Mat. 128 (2010) 108–114.
[8] Q. Tang, H. Xu, Y. Zheng, J. Wang, H. Li, J. Zhang, Catalytic dehydration of methanol to dimethyl ether over micro–mesoporous ZSM-5/MCM-41 composite molecular sieves, Appl. Catal. Gen. 413–414 (2012) 36–42.
[9] Y.N. Kochkin, N.V. Vlasenko, N.V. Kasian, O.V. Shvets, Effect of the acidity of Ca,H-Bea zeolites on their catalytic characteristics in the dimethyl ether production from methanol, Theor. Exp. Chem. 51 (2015) 327–332.
[10] P. Pérez-Uriarte, M. Gamero, A. Ateka, M. Díaz, A.T. Aguayo, J. Bilbao, Effect of the acidity of HZSM-5 zeolite and the binder in the DME transformation to olefins, Ind. Eng. Chem. Res. 55 (2016) 1513–1521.
[11] S.D. Kim, S.C. Baek, Y.-J. Lee, K.-W. Jun, M.J. Kim, I.S. Yoo, Effect of γ-alumina content on catalytic performance of modified ZSM-5 for dehydration of crude methanol to dimethyl ether, Appl. Catal. Gen. 309 (2006) 139–143.
[12] A.A. Rownaghi, F. Rezaei, M. Stante, J. Hedlund, Selective dehydration of methanol to dimethyl ether on ZSM-5 nanocrystals, Appl Catal. B Environ. 119–120 (2012) 56–61.
[13] Y. Fu, T. Hong, J. Chen, A. Auroux, J. Shen, Surface acidity and the dehydration of methanol to dimethyl ether, Thermochim. Acta. 434 (2005) 22–26.
[14] Q. Zhu, J.N. Kondo, R. Ohnuma, Y. Kubota, M. Yamaguchi, T. Tatsumi, The study of methanol-to-olefin over proton type aluminosilicate CHA zeolites, Microporous Mesoporous Mat. 112 (2008) 153–161.
[15] T. Yokoi, M. Yoshioka, H. Imai, T. Tatsumi, Diversification of RTH-type zeolite and its catalytic application, Angew. Chem. Int. Ed. 48 (2009) 9884–9887.
[16] D. Masih, H. Imai, T. Yokoi, J.N. Kondo, T. Tatsumi, Methanol conversion to lower olefins over RHO type zeolite, Catal. Commun. 37 (2013) 1–4.
[17] H. Robson, K. Lillerud, Contributors, in: Verified Synth. Zeolitic Mater, Elsevier Science, Amsterdam, 2001, pp. 8–17.
[18] H.-Y. Jeon, C.-H. Shin, H.J. Jung, S.B. Hong, Catalytic evaluation of small-pore molecular sieves with different framework topologies for the synthesis of methylamines, Appl. Catal. 305 (2006) 70–78.
[19] Y. Ji, J. Birmingham, M.A. Deimund, S.K. Brand, M.E. Davis, Steam-dealuminated, OSDA-free RHO and KFI-type zeolites as catalysts for the methanol-to-olefins reaction, Microporous Mesoporous Mat. 232 (2016) 126–137.
[20] D.M. Sung, Y.H. Kim, E.D. Park, J.E. Yie, Correlation between acidity and catalytic activity for the methanol dehydration over various aluminum oxides, Res. Chem. Intermed. 36 (2010) 653–660.
[21] M. Migliori, A. Aloise, E. Catizzone, G. Giordano, Kinetic analysis of methanol to dimethyl ether reaction over H-MFI catalyst, Ind. Eng. Chem. Res. 53 (2014) 14885–14891.
[22] E. Catizzone, A. Aloise, M. Migliori, G. Giordano, Dimethyl ether synthesis via methanol dehydration: effect of zeolite structure, Appl. Catal. Gen. 502 (2015) 215–220.
[23] Y. Wei, P.E. de Jongh, M.L.M. Bonati, D.J. Law, G.J. Sunley, K.P. de Jong, Enhanced catalytic performance of zeolite ZSM-5 for conversion of methanol to dimethyl ether by combining alkaline treatment and partial activation, Appl. Catal. Gen. 504 (2015) 211–219.
[24] S.-C. Baek, Y.-J. Lee, K.-W. Jun, S.B. Hong, Influence of catalytic functionalities of zeolites on product selectivities in methanol conversion, Energy Fuels 23 (2009) 593–598.